Chinese Chemical Letters 32 (2021) 3787–3792

Contents lists available at ScienceDirect

Chinese Chemical Letters

journal homepage: www.elsevier.com/locate/cclet

Communication

Polydopamine-mediated synthesis of Si@carbon@graphene aerogels for enhanced lithium storage with long cycle life

Ningning Li[a], Yi Liu[a], Xiaoyu Ji[a], Jiaxin Feng[a], Kai Wang[a], Jiayue Xie[a], Guanglu Lei[a], Xianghong Liu[a,b,*], Xiangxin Guo[a], Jun Zhang[a]

[a] College of Physics, Qingdao University, Qingdao 266071, China
[b] Key Laboratory of Advanced Energy Materials Chemistry (Ministry of Education), Nankai University, Tianjin 300071, China

ARTICLE INFO

Article history:
Received 17 March 2021
Revised 12 April 2021
Accepted 15 April 2021
Available online 26 April 2021

Keywords:
Si anode
Carbon coating
Graphene
Aerogel
Cycle life

ABSTRACT

The application of Si as the anode materials for lithium-ion batteries (LIBs) is still severely hindered by the rapid capacity decay due to the structural damage caused by large volume change (> 300%) during cycling. Herein, a three-dimensional (3D) aerogel anode of Si@carbon@graphene (SCG) is rationally constructed *via* a polydopamine-assisted strategy. Polydopamine is coated on Si nanoparticles to serve as an interface linker to initiate the assembly of Si and graphene oxide, which plays a crucial role in the successful fabrication of SCG aerogels. After annealing the polydopamine is converted into N-doped carbon (N-carbon) coatings to protect Si materials. The dual protection from N-carbon and graphene aerogels synergistically improves the structural stability and electronic conductivity of Si, thereby leading to the significantly improved lithium storage properties. Electrochemical tests show that the SCG with optimized graphene content delivers a high capacity (712 mAh/g at 100 mA/g) and robust cycling stability (402 mAh/g at 1 A/g after 1500 cycles). Furthermore, the full cell using SCG aerogels as anode exhibits a reversible capacity of 187.6 mAh/g after 80 cycles at 0.1 A/g. This work provides a plausible strategy for developing Si anode in LIBs.

Rechargeable LIBs have been widely used in portable electronic products, electric vehicles (EVs) and large-scale power grids [1,2]. However, the current commercial anode, *i.e.*, graphite materials, is greatly constrained by its theoretical specific capacity (372 mAh/g) and cannot meet the ever-increasing demands for high energy batteries [3,4]. Therefore, it is very imperative to develop anode materials with higher energy density and long cycle life. Silicon (Si) has been deemed as one of the most promising anode materials to replace the commercial graphite materials due to its relatively low working potential (~0.4 V *vs.* Li^+/Li), environmental benignity, high natural abundance and superior theoretical capacity of 4200 mAh/g [5–7].

However, the large volume change (> 300%) caused by the alloying/dealloying reactions of Si and Li will lead to the pulverization and structure breakage of the electrode materials, as well as the unstable formation of the solid electrolyte interphase (SEI) films on the electrode surface [8,9]. In addition, the low electronic conductivity also limits the practical application of Si anode [10]. Many ways have been explored to alleviate these critical issues by, *e.g.*, constructing appropriate nanostructures or encapsulating Si materials with various conductive carbon materials. Evidence has shown that nano-structuring of Si has successfully improved the physical and chemical properties including shortening the Li^+ diffusion path, increasing the contact area of the electrolyte and the electrode, and alleviating the stress caused by volume expansion [4,11,12]. Alternatively high capacity and stable cycling performance of Si can also be obtained by encapsulating Si with conductive carbon materials [13,14]. The improvement is resultant from the elastic properties and high conductivity of carbons [15].

Graphene aerogel (GA) with a 3D structure crosslinked by graphene nanosheets can afford high mechanical stability to strengthen the structural stability of electrodes [16]. The unique porous architecture of GA avoids the stacking of graphene sheets, contributes to the migration and diffusion of lithium ions and electrolyte, and provides enough space to adapt the large volume change [17,18]. These unique advantages make GA an ideal matrix

* Corresponding author at: College of Physics, Qingdao University, Qingdao 266071, China.
E-mail address: xianghong.liu@qdu.edu.cn (X. Liu).

https://doi.org/10.1016/j.cclet.2021.04.029
1001-8417/

for Si materials. However, the interaction between pristine Si and graphene sheets is too weak to guarantee the stability of the hybrid structure. In addition, the homogenous dispersion of Si within 3D GA to avoid aggregation of Si nanoparticles has been a challenge [19].

Herein, we designed a 3D SCG aerogel structure, in which N-carbon coated Si nanoparticles were uniformly fixed in the graphene aerogel. Polydopamine (PDA) serves as both the hydrogen-bond agent to attach Si on graphene and the precursor for the N-carbon coatings. PDA coating is necessary for the final formation of homogeneous 3D SCG aerogels. Benefiting from the dual protection from the functional N-carbon coatings and the 3D graphene structure, the SCG aerogel exhibits superior electrochemical properties in comparison to pristine Si materials, including high capacity (712 mAh/g at 0.1 A/g after 100 cycles) and long cycle stability with high capacity retention (402 mAh/g at 1 A/g after 1500 cycles). For demonstration, a full cell using SCG aerogels and commercial NCM622 as the anode and cathode is assembled, which displays a reversible capacity of 187.6 mAh/g after 80 cycles at 0.1 A/g and can successfully light up the LED arrays.

In this work, Si powder, dopamine hydrochloride (DA), graphene oxide (GO) and L-ascorbic acid (VC) were purchased and used directly without any treatment (Sinopharm Chemical Reagent Co., Ltd.). First, 400 mg of Si nanoparticles was added to 200 mL of Tris-buffer solution and dispersed by sonication for 30 min. Then, 200 mg of DA was added to the mixture and stirred for 12 h to obtain polydopamine-coated Si nanoparticles (Si@PDA). After washing and freeze-drying, the Si@PDA materials were annealed in Ar at 700 °C for 2 h to obtain SC sample.

In addition, GO suspension (6 mL, 5 mg/mL) and an appropriate amount of Si@PDA powder were added to 9 mL of water/ethanol (1:2 vol%) mixed solution with stirring, and then sonicated for 1 h. After that, VC (240 mg) was added to the mixture with stirring and kept at 80 °C for 8 h to form a hydrogel. Finally, the SCG aerogel was obtained after freeze-drying the hydrogel for 12 h and thermal annealing under the same conditions as above. The samples was named as SCG-x (x = 1, 2 and 3), where x denotes the different mass ratios of Si@PDA:GO of 1:1, 2:1 and 3:1, respectively. For comparison, GA and Si@graphene (SG) samples were prepared by the same process, except that Si@PDA was not added or was replaced by Si.

After the preparation of the samples, their physical and chemical properties were characterized by various methods. Raman spectra was obtained using Renishaw RM2000 with a laser wavelength of 532 nm. X-ray diffraction (XRD, Rigaku Smartlab) was investigated to determine the phase structure of the samples. Transmission electron microscope (TEM) and scanning electron microscope (SEM) were carried out on Carl Zeiss SIGMA 300 and FEI JEM2010, respectively. Energy dispersive X-ray spectroscopy (EDX) elemental mapping and high-resolution transmission electron microscope (HRTEM) were conducted using FEI Tecnai G2 F20 with an acceleration voltage of 200 kV. Fourier transform-infrared (FT-IR) spectra and X-ray photoelectron spectroscopy (XPS) were recorded on Thermo scientific (Nicolet iz10) and Thermo ESCALAB 250, respectively, and 284.8 eV was used as the reference for carbon. Thermogravimetric analysis (TGA, TG209, NETZSCH) be used to determine the mass ratio in the nanocomposite.

In addition, electrochemical tests were performed with CR2025 coin-type cells assembled in an Ar-filled glove box (O_2, H_2O < 0.1 ppm, Mikrouna, China). A mixture of active material, super P and polyvinylidene fluoride (PVDF) with a weight ratio of 8:1:1 was coated on copper foil to prepare the working electrode. The loading density of the electrode material SCG is about 0.8–1 mg/cm^2. In the assembled cells, fresh lithium foil, glass fiber membrane and 1 mol/L $LiPF_6$ in DMC/EMC/EC (1:1:1, v/v/v) were used as reference electrode, current separator and electrolyte, respectively. Galvanostatic cycling tests were performed on the Land CT2001A battery testing system at a potential range of 0.01–3.0 V at room temperature. Cyclic voltammetry (CV) curves and electrochemical impedance spectroscopy (EIS) tests were performed on an electrochemical workstation (VSP, Bio-Logic). In detail, the frequency range of the EIS tests were 10^{-3}–10^5 Hz. The potential range and scan rate of the CV were 0.01–3.0 V and 0.1 mV/s, respectively.

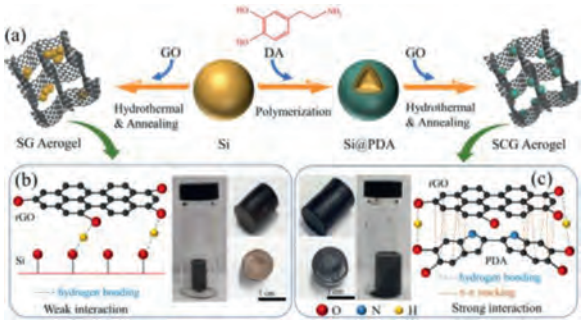

Fig. 1. (a) Schematic illustration of the PDA-mediated assembly process for synthesis of SG and SCG aerogel; schematic bonding interactions and digital graphs of (b) Si/rGO and (c) Si@PDA@rGO hydrogel.

The synthesis process of 3D SCG aerogel is shown in Fig. 1a. PDA is coated on Si nanoparticles due to the hydrogen bonding interaction between the surface hydroxyl of Si and the phenolic hydroxyl of DA [20]. In addition, the PDA coating is necessary for the formation of homogenous Si@PDA@reduced graphene oxide (Si@PDA@rGO) hydrogel due to the hydrogen bonding, chemical cross-linking and π-π stacking between PDA and rGO [21,22]. These abundant bondings endow a strong interaction, which leads to the successful synthesis of Si@PDA@rGO hydrogel. In the control experiments without using PDA, as shown in Fig. 1b, it is noted that although graphene hydrogel can form successfully, the Si nanoparticle are gathered at the bottom due the weak interaction between Si and rGO. In contrast, no precipitates can be observed in Fig. 1c, indicating Si@PDA nanoparticles have been successfully embedded in the 3D graphene hydrogel. Finally, after freeze-drying and annealing, the Si@PDA@rGO hydrogel is converted into SCG aerogel. In particular, the PDA coating is converted into a N-doped carbon coating, which can avoid contact between Si and electrolyte, enhance the Li^+ storage performance and reduce the generation of SEI film. The carbon coating and the 3D graphene aerogel structure in SCG can improve the electronic conductivity, effectively avoid the aggregation of Si nanoparticles, and adapt to the large volume change of Si during the repeated charging and discharging. Therefore, the SCG provides the possibility of achieving long cycle life and good capacity.

The composition of the samples has been determined by XRD, Raman, FT-IR, TGA and XPS. As shown in Fig. S1a (Supporting information), the XRD patterns of Si, SC, SG and SCG show sharp diffractions at 28.4°, 47.3°, 56.1° and 69.1°, which correspond to the (111), (220), (311) and (400) planes of Si (PDF# 89–2955), respectively [23,24]. Meanwhile, the weak diffractions at 22.0° of SC and 25.8° of GA belong to amorphous carbon and graphene, proving the existence of carbon coating and graphene in SCG [25,26]. According to the Raman spectra (Fig. S1b in Supporting information), the characteristic band of Si (513.2 cm^{-1}) further indicates the presence of Si in SCG. In addition, the signals appearing at 1346.7 and 1590.5 cm^{-1} correspond to the D band and the G band

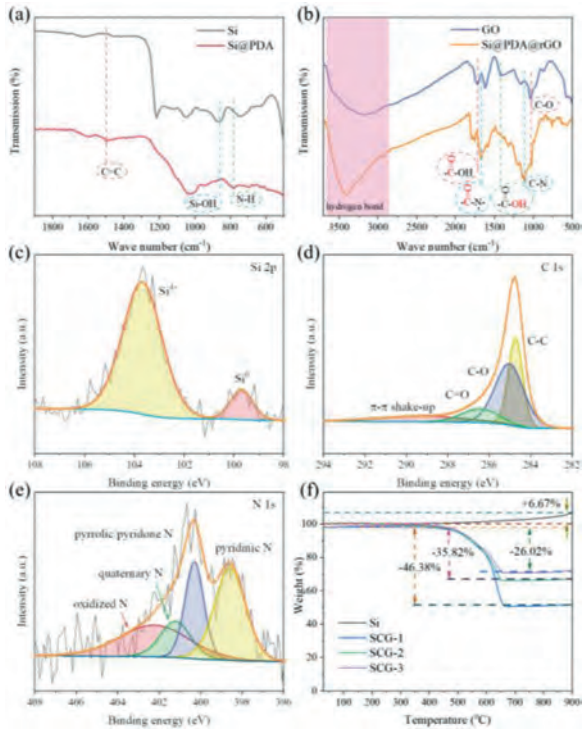

Fig. 2. FT-IR spectra of (a) Si and Si@PDA, (b) GO and Si@PDA@rGO. High resolution XPS spectra of (c) Si 2p, (d) C 1s and (e) N 1s in SCG-2. (f) TGA curve of Si, SCG-1, SCG-2 and SCG-3.

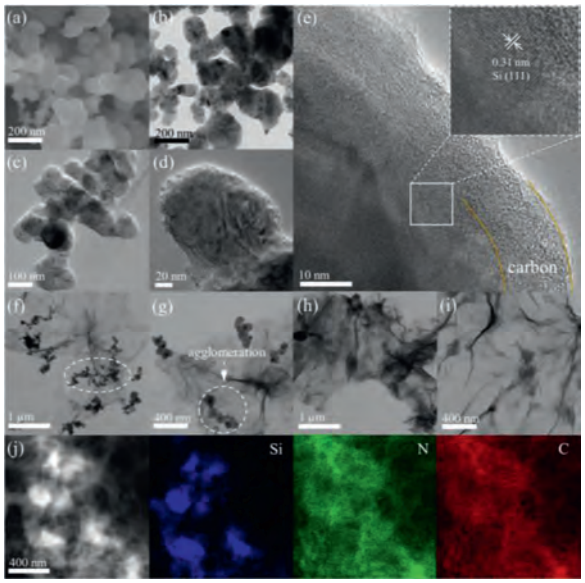

Fig. 3. (a) SEM and (b) TEM images of Si. (c, d) TEM and (e) HRTEM images of SC. TEM images of (f, g) SG and (h, i) SCG-2. (j) HAADF-STEM and EDX of SCG-2 with corresponding elemental mapping of Si, N and C.

of carbon [5,13]. High degree of graphitization ($I_D/I_G < 1$) in SCG-2 is beneficial to enhance the electronic conductivity of electrode materials, as well as the disordered graphitic structure may contribute to the diffusion and transportation of Li^+.

FT-IR spectra were used to determine the bonding chemistry of in the samples. As shown in Fig. 2a, the broad peak at 850 cm^{-1} in the FT-IR spectra of Si is related to the asymmetric vibration of Si-OH [27], and it disappears in Si@PDA. In addition, the bands at 1508 and 790 cm^{-1} of Si@PDA are related to the vibrations of the C=C bond and the N–H bond, respectively, which indicates that the PDA coating is coated on the Si nanoparticles through hydrogen bonding [20,21]. In Fig. 2b, the peak representing the stretching vibration of C–O (1043 cm^{-1}) appears in GO, while it almost disappears in Si@PDA@rGO, which means that GO is reduced to rGO during the hydrothermal self-assembly process. As shown in the FT-IR spectra of GO, the broad band centered on 3186 cm^{-1} is attributed to the hydrogen bond between carboxyl groups, while the peaks at 1722 and 1410 cm^{-1} belong to the vibrations of C=O and O–H bond of carboxyl group [28]. However, these bonds related to carboxyl groups in GO and the N–H bond in Si@PDA are replaced by bands at 3410 and 1674 cm^{-1} in Si@PDA@rGO, which represent the hydrogen bonds (N–H/O–H or O–H/O−H) and the C=O vibration of amide between PDA and rGO, respectively [21,29]. Furthermore, the latter proves the existence of chemical cross-linking. In addition, as shown in Fig. 2c, the π-π stacking between rGO and PDA is also beneficial to the formation of homogenous Si@PDA@rGO hydrogel [22,30]. The above results further support the bonding interactions shown in Fig. 1.

The structure of 3D aerogel and the dispersion of Si nanoparticles were observed by SEM. In Fig. S2 (Supporting information), both SG and SCG-2 exhibit a hierarchical structure, which is typical of graphene aerogel [31,32]. The Si nanoparticles are observed to severely agglomerate in SG (Figs. S2a and b), as indicated by the white circles. In contrary, the Si nanoparticles are homogeneously wrapped in graphene in SCG-2 (Fig. S2c and d). The uniform dispersion of Si nanoparticles in SCG-2 benefits from the crucial role of the PDA coating. As shown by the results of FT-IR (Figs. 2a and b), the Si@PDA and graphene sheets are firmly connected by hydrogen bonding, chemical cross-linking and π-π stacking. Therefore, Si@PDA can be uniformly dispersed and enveloped by graphene sheets in SCG −2, instead of agglomeration in SG. According to the digital graphs (Fig. 1b), SEM (Figs. S2a and b) and TEM images (Figs. 3f and g), if there is no PDA coating, Si nanoparticles cannot be uniformly distributed on the graphene sheets.

XPS was used to explore the chemical states of elements in SCG-2. As shown in Fig. 2c, the high resolution XPS spectrum of Si 2p shows that there are two valence states of Si, *i.e.*, Si^{4+} (103.7 eV) and Si^0 (99.7 eV) [23]. The presence of Si^{4+} is ascribed to the oxidized surface layer of SiO_2, thereby providing the hydroxyl (-OH) interconnected with DA [20]. In Fig. 2d, the high resolution XPS spectrum of C 1s shows four peaks at 289.3, 286.6, 285.2 and 284.8 eV, corresponding to the π-π shakeup, C=O, C−O and C−C bonds, respectively [13,33–35]. These carbon-oxygen bonds suggest successful coating of carbon on Si nanoparticles. The high resolution XPS spectra of N 1s is deconvoluted into four peaks at 398.6, 400.2, 401.3 and 402.5 eV (Fig. 2e), representing pyridinic N, pyrrolic/pyridone N, quaternary N and oxidized N, respectively [14]. Nitrogen doping in the carbons can improve the lithium storage performance by promoting electrochemical reactions through creating more defects and increasing active sites for Li^+ adsorption [26,36,37].

The content of each component and thermal properties of SCG-2 have been determined by TGA. As displayed in Fig. 2f, the weight loss before 200 °C is attributed to the evaporation of water in the sample, while the weight change from 200 °C to 900 °C corresponds to the oxidation of Si and the combustion of carbon and graphene [14,37,38]. The Si contents in SCG-1, SCG-2 and SCG-3 sample can be roughly evaluated, assuming the Si component in these samples are fully oxidized in the TGA curves. As a result, the contents of Si in SCG-1, SCG-2 and SCG-3 sample are approximately

49.42, 59.52 and 68.88%, respectively. In addition, the content of carbon and graphene in SCG-2 is calculated to be about 40.48%.

The microstructure of the samples was further investigated by TEM and HRTEM. As shown in Figs. 3a and b, the Si nanoparticles used in the prepared samples have a diameter of 100–200 nm, and they are severely agglomerated together. Since there is no isolation of graphene, the PDA coating of SC forms an interconnected carbon layer after annealing (Figs. 3c and d). In addition, according to the HRTEM image of SC (Fig. 3e), the inter-planar spacing of 0.31 nm is related to the (111) plane of Si, and the thickness of the carbon coating is about 10 nm [13]. In the SG sample (Figs. 3f and g), Si nanoparticles agglomerated together and simply mixed with graphene without forming a stable structure. This result is consistent with the conclusion obtained from the SEM images (Figs. S2a and b) and the digital graph of Si/rGO hydrogel (Fig. 1a). However, in the SCG sample (Figs. 3h and i), the carbon-coated Si nanoparticles are tightly wrapped by graphene and are evenly dispersed in graphene aerogel, which matches the results of the SEM images (Figs. S2c and d). The HAADF-STEM image of SCG-2 (Fig. 3j) can prove that the Si nanoparticles coated with nitrogen-doped carbon are uniformly dispersed in the graphene aerogel structure.

By comparing the digital graph of Si/rGO hydrogel and Si@PDA@rGO hydrogel (Figs. 1b and c), as well as the SEM (Fig. S2) and TEM images (Figs. 3f–i) of SG and SCG-2, it can be found that the PDA coating can effectively avoid theagglomeration of Si nanoparticles and make them uniformly dispersed in the aerogel. This is because the PDA coating can be attached to Si nanoparticles through hydrogen bonding, and connected to rGO by hydrogen bonding, chemical cross-linking and π-π stacking (FT-IR spectra in Figs. 2a and b). It is worth noting that this is also essential for forming a stable structure.

Based on the above results, it can be confirmed that the 3D SCG structure has been successfully prepared, in which Si nanoparticles coated with N-doped carbon are uniformly fixed in the graphene aerogel.

The prepared samples were used as anodes for LIBs to explore their electrochemical behavior. Fig. 4a shows the CV curves for the first five scans and of SCG-2. The broad reduction peak from 0.9 V to 0.2 V that only appeared in the first scan is related to the formation of a stable SEI film [39]. The sharp reduction peak at 0.01 V represents the lithiation of Si to form Li_xSi, while the two distinct oxidation peaks at 0.36 and 0.51 V are attributed to the extraction of Li^+ from Li_xSi alloy [10,14,40]. As the subsequent scans progress, the area and intensity of the oxidation peaks increase gradually, which may be due to the activation of the electrode materials [41]. As shown in Fig. 4b, the charge/discharge profiles of the SCG-2 can be well matched with the CV curves. The plateau of the 1st discharge curve at 0.1 V is related to the reduction peak of the CV curve at 0.01 V, which represents the lithiation of crystalline Si. In the subsequent discharge curves, this plateau appears at about 0.3 V due to the conversion of crystalline Si to amorphous Si after the lithiation/de-lithiation process, which is also the reason for the change in the intensity of reduction peak (Fig. 4a) [42–44]. In addition, the long slope between 3.0 and 0.3 V in the discharge curves may represent the lithiation of graphene [14], while the gentle slope between 0.3 V and 0.5 V in the charge curves is related to the de-lithiation of Li_xSi [45]. In the first cycle of SCG-2 (Figs. 4b and d), the charge and discharge specific capacities are 1244.3 and 1618.1 mAh/g, respectively. Its first cycle coulombic efficiency is 76.90%, which is higher than SCG-1 (56.97%) and SCG-3 (58.58%) (Fig. S3 in Supporting information).

As shown in Fig. S3 and Fig. 4c, SCG-2 has better capacity performance than SCG-1 and SCG-3, *i.e.*, 712 mAh/g at 0.1 A/g after 100 cycles and 402 mAh/g at 1 A/g after 1500 cycles. The phenomenon that the specific capacity rises first and then decreases as the Si content in the SCG sample increase may be due to the low Si content in SCG-1 limits its capacity increase, while the excessive Si content in SCG-3 causes the structure to not stable. Therefore, the appropriate specific gravity of Si@C and graphene in SCG-2 can ensure a higher capacity while maintaining the structural stability of the aerogel. Compared to Si and SG, the coulombic efficiency of SCG-2 is close to 100% and remains stable after a short activation process (Fig. 4d), showing excellent cycling stability. In addition, comparing SCG-2 with other samples (Figs. 4d and e), it can be found that SCG-2 far exceeds the Si, SC and SG samples in reversible capacity and cycle stability. This is mainly attributed to the multiple effects of the N-carbon coating: (1) provide a large number of electrically contact points to enhance the electronic conductivity of the electrode; (2) separate the electrolyte and Si to reduce the consumption of electrolyte and active materials and suppress the formation of SEI film; (3) inhibit and buffer the large volume change of Si and limit its aggregation. GA has extremely excellent cycle stability and can provide a stable structure for composite materials. Whether Si nanoparticles are compounded with carbon or graphene, they have a significant improvement in capacity performance, but their cycle stability is poor (Fig. 4e). Therefore, the SCG-2 sample, *i.e.*, appropriate proportion of Si nanoparticles coated with N-doped carbon are fixed in 3D graphene aerogel, can effectively improve the electrochemical performance, which is mainly due to the double protection provided by the carbon coating and the graphene aerogel structure. In addition, we summarize and compare the lithium storage properties of some Carbon-based Si/SiO_x electrodes. As shown in Table S1 (Supporting information), the performance of SCG-2 sample is superior to other electrodes in terms of long cycle life.

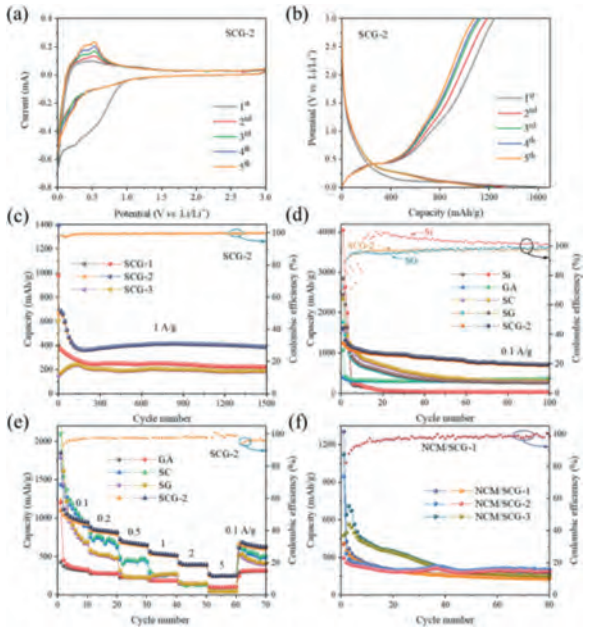

Fig. 4. (a) CV curves and (b) charge/discharge voltage profiles for cycles at a current density of 0.1 A/g of the SCG-2. (c) Cycling properties at a current density of 1 A/g of the SCG-1, SCG-2 and SCG-3. (d) The cycling properties at a current density of 0.1 A/g. (e) Rate performances of the Si, SC, SG and SCG-2 for the half cell. (f) Specific capacity for cycles at 0.1 A/g of the NCM/SCG-1, NCM/SCG-2 and NCM/SCG-3 full cell.

EIS further clarifies the potential causes of the excellent electrochemical performance of SCG-2 electrode. In Fig. S4 (Supporting information), the Nyquist plots consist of a slope curve at low frequency and a semicircle at the high and medium frequency, respectively representing the diffusion of Li^+ in the solid electrode

and the charge-transfer resistance at the interface between the electrolyte and the electrode [46–48]. It can be seen that both the diameter of the semicircle and the slope of the slope curve of the SCG-2 are smaller than that of the Si, which means that the SCG-2 has a smaller charge-transfer resistance and a larger diffusion coefficient of Li^+. This is because the nitrogen-doped carbon coating and graphene aerogel structure in SCG-2 can effectively improve the electronic conductivity and lithium ion diffusion rate [49,50].

The influence of repeated charging and discharging process on the stability of electrode structure was studied by TEM. After 100 cycles at a current of 0.1 A/g, SCG-2 electrode still maintains the stable structure before cycling, and the Si nanoparticles are tightly wrapped by graphene sheets (Fig. S5b in Supporting information). However, as shown in Fig. S5a (Supporting information), Si nanoparticles in the SG electrode are separated from the graphene, severely aggregated and broken. Therefore, the stable structure can endow SCG-2 electrode with excellent electrochemical performance, which matches the results of the cycling test in Fig. 4.

To explore the potential of the SCG aerogels for practical applications, the SCG-2 anode and commercial NCM622 cathode were used to assemble a full cell (named as NCM/SCG). The electrolyte used in the full cell is same as that used in the half cell, that is, 1 mol/L $LiPF_6$ in DMC/EMC/EC (1:1:1, v/v/v). According to the charge/discharge voltage profiles of SCG-2 half cell and NCM622 half cell (Fig. S6a in Supporting information), the working voltage range of NCM/SCG full cell is set to 2.5–4.35 V. In order to explore the influence factors of electrochemical performance, the SCG-2 anodes used to assemble NCM/SCG-1, NCM/SCG-2 and NCM/SCG-3 are respectively treated as follows in half cell before the full cell is assembled: pre-lithiation, completing 300 cycles charge/discharge at 1 A/g (the performance of the SCG-2 anode material has been stable under this condition in Fig. 4c) or using more PVDF binder when preparing the working electrode (SCG-2:super P:PVDF = 8:0:2).

As shown in Fig. S6b (Supporting information), the reversible capacity of commercial NCM622 half-cell is very stable and even increases with the activation of active materials, therefore does not cause the performance degradation of the full cell. In Fig. 4f, the NCM/SCG-1 full cell has a relatively stable performance after a large attenuation in the first 40 cycles, and exhibits a reversible capacity of 131.1 mAh/g after 80 cycles at 0.1 A/g. The specific capacities of the NCM/SCG-2 and NCM/SCG-3 remained 187.6 and 154.3 mAh/g after 80 cycles, respectively. More importantly, their specific capacity attenuation is better than that of NCM/SCG-1. It may be because the structure of the NCM/SCG-2 anode has been adjusted after a long cycle in the half cell, and the final stable SEI film has been formed on the electrode surface, which reduces the consumption of electrolyte and the reduction of capacity. In addition, by comparing the capacity attenuation in Fig. 4f, it can be seen that more PVDF binder in the NCM/SCG-3 anode can effectively inhibit or delay the shedding of the active material. Therefore, it can be inferred that the attenuation of NCM/SCG-1 full cell is not only related to the consumption of electrolyte [51], but also due to the structural adjustment and partial shedding of active material in SCG-2 anode. Furthermore, as shown in Fig. S6c (Supporting information), the NCM/SCG full cell can successfully light up the red light emitting diode (LED, standard operating power 0.02 W) arrays, which proves its prospect towards real application.

In summary, a 3D SCG aerogel structure has been rationally designed by a PDA-assisted assembly strategy. The chemical interaction between PDA and the oxygen-containing groups of GO is the key to the formation of homogeneous SCG aerogels. The N-doped carbon coating and graphene aerogel structure synergistically solve the problems of poor electronic conductivity and crushing and shedding of electrode material caused by large volume change during repeated charge and discharge. Therefore, the SCG aerogels shows much better electrochemical performance than Si and SC in terms of specific capacity, rate performance and cycle stability. A full cell was also assembled to explore its practical potential of the as-designed SCG aerogels. The proposed strategy and the excellent electrochemical properties delivered by the Si composites suggest a feasible protocol to synthesize high performance Si-based anodes for future LIBs.

Declaration of competing interest

The authors declare that they have no known competing financial interests or personal relationships that could have appeared to influence the work reported in this paper.

Acknowledgments

This work is financially supported by the National Natural Science Foundation of China (Nos. 51972182 and 61971252), the Shandong Provincial Natural Science Foundation (Nos. ZR2020JQ27 and ZR2019BF008), the Youth Innovation Team Project of Shandong Provincial Education Department (No. 2020KJN015).

Supplementary materials

Supplementary material associated with this article can be found, in the online version, at doi:10.1016/j.cclet.2021.04.029.

References

[1] M. Li, J. Lu, Z.W. Chen, K. Amine, Adv. Mater. 30 (2018) 1800561.
[2] D. Castelvecchi, E. Stoye, Nature 574 (2019) 308.
[3] J.B. Goodenough, K.S. Park, J. Am. Chem. Soc 135 (2013) 1167–1176.
[4] H. Wu, G.H. Yu, L.J. Pan, et al., Nat. Commun 4 (2013) 1943.
[5] X.H. Liu, J. Zhang, W.P. Si, et al., ACS Nano 9 (2015) 1198–1205.
[6] K. Feng, M. Li, W.W. Liu, et al., Small 14 (2018) 1702737.
[7] P. Li, J.Y. Hwang, Y.K. Sun, ACS Nano 13 (2019) 2624–2633.
[8] Y.Y. Zhang, G.W. Hu, Q. Yu, et al., Mat. Chem. Front. 4 (2020) 1656–1663.
[9] X.H. Shen, Z.Y. Tian, R.J. Fan, et al., J. Energy Chem. 27 (2018) 1067–1090.
[10] Z. Benzait, N. Yuca, Electrochim. Acta 339 (2020) 135917.
[11] S.H. Ng, J.Z. Wang, D. Wexler, et al., Angew. Chem. Int. Ed. 45 (2006) 6896–6899.
[12] Y. Yang, W. Yuan, W.Q. Kang, et al., Sustain. Energ. Fuels 4 (2020) 1577–1594.
[13] Y. Yang, H.X. Yang, Y.Q. Wu, et al., Electrochim. Acta 341 (2020) 136037.
[14] W. Sun, L. Wan, X.C. Li, X.H. Zhao, X.B. Yan, J. Mater. Chem. A 4 (2016) 10948–10955.
[15] Y.Z. Zhou, Y.J. Yang, G.L. Hou, et al., Nano Energy 70 (2020) 104568.
[16] G.J. Hu, C. Xu, Z.H. Sun, et al., Adv. Mater. 28 (2016) 1603–1609.
[17] C.P. Yuan, Q. Wu, Q. Li, et al., ACS Sustain. Chem. Eng. 6 (2018) 8392–8399.
[18] X. Zhang, J. Zhou, Y.Y. Zheng, D.Y. Chen, J. Power Sources 439 (2019) 227112.
[19] H. Shan, X.F. Li, Y.H. Cui, et al., Electrochim. Acta 205 (2016) 188–197.
[20] Y. Bie, J. Yang, X. Liu, J. Wang, et al., ACS Appl. Mater. Interfaces 8 (2016) 2899–2904.
[21] D.A. Agyeman, K. Song, G.H. Lee, M.h. Park, Y.M. Kang, Adv. Energy Mater. 6 (2016) 1600904.
[22] S. Wang, C.Y. Duan, W.Z. Yang, et al., Nanoscale 12 (2020) 11936–11946.
[23] Q. Ma, H.W. Xie, J.K. Qu, et al., ACS Appl. Energ. Mater. 3 (2019) 268–278.
[24] J. Li, J.Y. Yang, J.T. Wang, S.G. Lu, Rare Metals 38 (2017) 199–205.
[25] K. Wang, N.N. Li, J.Y. Xie, et al., Electrochim. Acta 372 (2021) 137863.
[26] X.H. Liu, J. Zhang, S.J. Guo, N. Pinna, J. Mater. Chem. A 4 (2016) 1423–1431.
[27] E.B. Lim, T.A. Vy, S.W. Lee, J. Mat. Chem. B 8 (2020) 2096–2106.
[28] L. Wang, D. Wang, Z. Dong, F. Zhang, J. Jin, Nano Lett. 13 (2013) 1711–1716.
[29] P. Gholami, A. Khataee, B. Vahid, Ind. Eng. Chem. Res. 59 (2020) 183–193.
[30] Y. Deng, X.Y. Gao, X.L. Shi, et al., Chem. Mat. 32 (2020) 2180–2193.
[31] M.A. Worsley, P.J. Pauzauskie, T.Y. Olson, et al., J. Am. Chem. Soc 132 (2010) 14067–14069.
[32] H. Hu, Z.B. Zhao, W. Wan, Y. Gogotsi, J.S. Qiu, Adv. Mater. 25 (2013) 2219–2223.
[33] J. Guo, G. Zhao, T. Xie, et al., ACS Appl. Mater. Interfaces 12 (2020) 19023–19032.
[34] C.L. Yan, Rare Metals 39 (2020) 458–459.
[35] K.C. Wasalathilake, S.N.S. Hapuarachchi, Y. Zhao, et al., ACS Appl. Energ. Mater. 3 (2019) 521–531.

[36] L. Sun, X.H. Liu, T.T. Ma, et al., Solid State Ion. 329 (2019) 8–14.
[37] T.T. Ma, X.H. Liu, L. Sun, et al., Electrochim. Acta 293 (2019) 432–438.
[38] X.H. Liu, T.T. Ma, L. Sun, et al., ChemSusChem 11 (2018) 1321–1327.
[39] R.S. Gao, J. Tang, X.L. Yu, et al., Nano Energy 70 (2020) 104444.
[40] Y.R. Ji, S.T. Weng, X.Y. Li, Q.H. Zhang, L. Gu, Rare Metals 39 (2020) 205–217.
[41] X.Q. Yuan, H.X. Xin, X.Y. Qin, et al., Electrochim. Acta 155 (2015) 251–256.
[42] Z.H. Wang, Y. Li, S.Z. Huang, et al., J. Mater. Chem. A 8 (2020) 4836–4843.
[43] C.H. Jung, J. Choi, W.S. Kim, S.H. Hong, J. Mater. Chem. A 6 (2018) 8013–8020.
[44] L.S. Wang, Y.Y. Fang, T. Zhao, et al., Rare Metals 39 (2020) 392–401.
[45] X.J. Bai, Y.Y. Yu, H.H. Kung, B. Wang, J.M. Jiang, J. Power Sources 306 (2016) 42–48.
[46] N.N. Li, L. Sun, K. Wang, et al., J. Energy Chem. 51 (2020) 62–71.
[47] L. Sun, T. Ma, J. Zhang, et al., Electrochim. Acta 321 (2019) 134672.
[48] T.T. Ma, X.H. Liu, L. Sun, et al., J. Energy Chem. 34 (2019) 43–51.
[49] Z.H. Wu, J.Y. Yang, B. Yu, et al., Rare Metals 38 (2016) 832–839.
[50] M.S. Balogun, W.T. Qiu, Y. Luo, et al., Nano Res 9 (2016) 2823–2851.
[51] P. Xiong, L. Peng, D.H. Chen, et al., Nano Energy 12 (2015) 816–823.